Investigations of single-wall carbon nanotube growth by time-restricted laser vaporization

Alex A. Puretzky,[1,2] Henrik Schittenhelm,[1] Xudong Fan,[1]* Michael J. Lance,[1] Larry F. Allard Jr.,[1] and David B. Geohegan[1]
[1]*Solid State Division, Oak Ridge National Laboratory, Oak Ridge, Tennessee 37831-6056*
[2]*Department of Materials Science and Engineering, University of Tennessee, Knoxville, Tennessee 37996-22100*
(Received 1 February 2002; published 24 June 2002)

The growth times of single-wall carbon nanotubes (SWNT's) within a high-temperature laser-vaporization (LV) reactor were measured and adjusted through *in situ* imaging of the plume of laser-ablated material using Rayleigh-scattered light induced by time-delayed, 308-nm laser pulses. Short SWNT's were synthesized by restricting the growth time to less than 20 ms for ambient growth temperatures of 760–1100 °C. Statistical analysis of transmission electron microscope photographs indicated most-probable lengths of 35–77 nm for these conditions. Raman spectra (E_{ex}=1.96 and 2.41 eV) of the short nanotubes indicate that they are well-formed SWNT's. The temperature of the particles in the vortex-ring-shaped plume during its thermalization to the oven temperature was estimated by collecting its blackbody emission spectra at different spatial positions inside the oven and fitting them to Planck's law. These data, along with detailed oven temperature profiles, were used to deduce a complete picture of the time spent by the plume at high growth temperatures (760–1100 °C). The upper and lower limits of the growth rates of SWNT's were estimated as 0.6 and 5.1 μm/s for the typical nanosecond Nd:YAG laser-vaporization conditions used in this study. These measurements permit the completion of a general picture of SWNT growth by LV based on imaging, spectroscopy, and pyrometry of ejected material at different times after ablation, which confirms our previous measurements that the majority of SWNT growth occurs at times greater than 20 ms after LV by the conversion of condensed phase carbon.

DOI: 10.1103/PhysRevB.65.245425 PACS number(s): 81.07.De, 81.16.Mk

I. INTRODUCTION

Single-wall carbon nanotubes (SWNT's) exhibit remarkable electronic and structural properties, which promise to revolutionize various application areas, from nanoscale electronics to ultralightweight structural materials.[1] Laser vaporization is one of the best methods to grow high-quality, high-purity SWNT's. As typically employed, each laser shot vaporizes a small amount of material ($\sim 10^{16}$ carbon atoms and $\sim 10^{14}$ metal catalyst atoms, e.g., ~1 at. % Ni, Co, Fe, Y, etc.) inside an oven (~1200 °C) into ~500 Torr of gently flowing inert gas.[2,3] On a single laser shot,[4] the ejected material self-assembles to form a high volume fraction of SWNT's, which can be up to 10 μm in length.[3,5]

Since the first introduction of laser-vaporization process in 1995,[2] researchers attempted optimization by manipulating numerous experimental variables, e.g., laser parameters (energy fluence, peak power, repetition rate, cw versus pulsed),[4,6–9] target composition,[10,11] carrier gas-flow rate and pressure,[7,12] ambient temperature,[7,13] etc.
These studies provided a reasonable optimization of the process and created many speculations about the growth mechanism.

Unfortunately, the growth of SWNT's is not controlled or fully understood. Thus their potential technological applications, which depend on the atomic-scale structure (chirality), growth rates and the possibility of large-scale production are affected by this lack of fundamental understanding.

The first attempts to perform *in situ* spectroscopic studies during SWNT growth were based on the observation of the luminous laser plasma at early times ($\Delta t < 80\ \mu$s) after nanosecond Nd:YAG laser ablation[14] and after long-pulse CO_2-laser vaporization at 25–1200 °C.[15] These measurements were limited to times when the ablated material was still quite hot.

Our approach to understanding the growth mechanism and optimizing the yield of SWNT's is to combine laser vaporization and *in situ* diagnostics.[16–18] Recently, we used laser-induced emission, gated intensified charge-coupled device (ICCD) imaging, and optical spectroscopy to probe the plume of ablated material during a long time interval ($0 < \Delta t <$ several seconds) after an 8-ns Nd:YAG-laser-ablation pulse.[16–18] Combined imaging and spectroscopy of Co atoms, C_2 and C_3 molecules, and clusters indicated that the atomic and molecular vapor quickly condensed into clusters and became trapped in aggregates within a vortex ring-shaped plume. The times for conversion of atomic and molecular species to clusters was estimated as ~200 μs for carbon and ~2 ms for cobalt at 1100 °C. We concluded that the majority of SWNT growth occurs within the spinning vortex ring, during its long propagation time within the hot oven, from the available feedstock of *condensed-phase* metal and carbon nanoparticles. This conclusion was strongly supported by our recent work where long SWNT's (μm in length) were grown by annealing nanoparticulate aggregates which were generated in the laser-vaporization apparatus, but were allowed only sufficient time to grow short SWNT's (<200 nm long). This material, which contained mostly amorphous carbon and metal nanoparticles, was collected and subjected to *ex situ*, high-temperature (950–1300 °C) annealing in order to verify that growth of SWNT's could proceed by the *condensed-phase conversion* mechanism at temperatures similar to those experienced by the nanoparticles in the vortex ring plume during laser vaporization.[19]

The main conclusions regarding plume composition versus time were later confirmed by Kokai *et al.*[20] who used a similar time-resolved imaging and spectroscopy approach

 ©2002 The American Physical Society

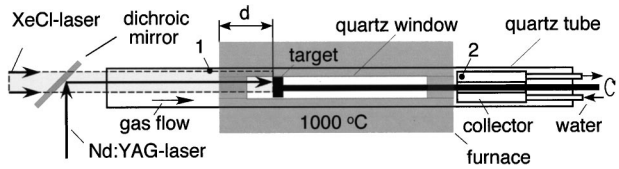

FIG. 1. Schematic of the 2-in-diam quartz tube and hot furnace with the viewing quartz window used for laser-vaporization growth of SWNT's with *in situ* laser-induced emission imaging diagnostic. Beam geometries are indicated. The black dots and the numbers show the collection points of the vaporized material: (1) upstream and (2) collector. The C/Ni/Co target was positioned at a distance $d=10$ cm from the front of the furnace.

based on *in situ* measurements of laser-induced emission and scattering from the propagating plume.

De Boer *et al.*[21] performed *in situ*, laser-induced fluorescence monitoring of the atomic Ni density in the near-target region ($d=1-3$ mm) and confirmed that the majority of Ni atoms also stay in the vapor phase for several milliseconds after ablation (consistent with our measurements on Co).[16–18]

Prior to these diagnostic studies very little was known about where, when, and at what rate the growth occurred. Even today, despite diagnostic investigations, estimates for growth rates of SWNT's produced by laser vaporization inside comparable hot oven environments range over five orders of magnitude, from $\sim$1 μm/s up to $\sim$15 cm/s.[22,23]

In this study we report the growth and characterization of short SWNT's (35–77 nm long) at three different oven temperatures. Detailed length characterizations of the short SWNT's are combined with *in situ* measurements of the growth time to provide new estimates of the growth rates. The short SWNT's are characterized by Raman spectroscopy and transmission electron microscopy (TEM). Detailed information on the growth environment of SWNT's during the early stages of their development is provided with new estimates of size and temperature of the aggregated nanomaterial which propagates inside the oven reactor a few milliseconds after laser vaporization. These measurements are correlated with oven temperature profiles and Rayleigh-scattering imaging of the propagating nanomaterial to restrict growth times available at known temperatures. Using length distributions of SWNT's produced under these well-defined conditions, the upper and lower limits of the growth rates of SWNT's were estimated as 0.6 and 5.1 μm/s for the typical nanosecond laser-vaporization conditions used in this study.

These results further support our previous studies which indicate that SWNT's grow over extended times (>100 ms to seconds) by a condensed phase conversion process. In conclusion, a comprehensive picture of SWNT growth is presented.

II. EXPERIMENT

The SWNT growth setup is shown in Fig. 1, and details are described in Refs. 17 and 18. It consists of a quartz tube (2-in. diameter, 24-in. length) mounted inside a hinged tube furnace (12-in. length) that can operate at maximum temperature of 1200 °C. The quartz tube was O-ring sealed to standard 4.5-in. conflat vacuum components. The ablation and probe laser beams entered the quartz tube through the same Suprasil window, which was mounted in a vacuum flange. A dichroic mirror was used to reflect the ablation laser beam while coaxially passing the probe laser beam. The furnace was equipped with a rectangular quartz window (10-in. length, 1-in. width, Suprasil 1) for spectroscopic diagnostics of the ablated material inside the furnace. A temperature profile along the axis of the quartz tube was measured by introducing a thermocouple coaxially with the quartz tube. In this case the Suprasil laser-entry window was replaced with a mount for the thermocouple. The end of the thermocouple could be positioned at any point at the tube axis.

Argon gas was introduced around the quartz laser-entry window at a flow rate of 100 sccm. The pressure was maintained at 500 Torr by pumping through a needle valve downstream of a brass water-cooled collector, which was inserted into the quartz tube and positioned just outside the furnace.

A 1-in.-diam target prepared from carbon cement (Dylon GC) was prepared to incorporate powders of Ni (Alfa, 2.2–3.0 μm, 99.9%) and Co (Alfa, 1–6 μm, 99.8%) such that the Ni and Co concentration resulted in 1 at. % each. The target was screwed onto a 0.25-in.-diam graphite rod and was rotated during operation. This rod was mounted along the tube axis through a hole in the collector.

The ablation laser [1.06 μm Nd:YAG, 300 mJ, 8 ns full width at half maximum (FWHM) pulse] beam was focused to a 4-mm-diam, donut-shaped spot on the target. The energy density at the target was about 3 J/cm^2. A gated ICCD-camera system (Princeton Instruments, 5-ns minimum gate, 200–820 nm spectral range) was used to perform scattering imaging of the ablation plume using a defocused XeCl-laser pulse (308 nm, 30 ns FWHM, 6 mJ/cm^2) at different time delays. The 5-ns ICCD gate was set to occur at the peak of the XeCl laser pulse.

Material collected from the chamber was investigated using Raman backscattering under ambient conditions in a microscope setup (Nachet NS400, 80×, N.A. 0.90) using $\sim$1 mW of 632.8-nm excitation ($\sim$3-μm-diam spot size) from a HeNe laser. The scattered light was passed through a spectrograph (HoloSpec f/1.8, Kaiser Optical Systems) and was detected with an ICCD camera (PI- MAX, Princeton Instruments). Raman spectra were also obtained with a Dilor XY800 triple-stage Raman microprobe (JY, Inc.) using a Coherent Innova 308 C Ar$^+$ laser (515-nm excitation, 1 mW in $\sim$2-μm spot size) power at the specimen.

III. GROWTH OF SHORT SWNT's

Growth rates of SWNT's were estimated by measuring length distributions of SWNT's grown for known durations inside the hot oven. However, reliable estimates of SWNT lengths can only be performed for short nanotubes where the ends of the nanotubes can be clearly determined in TEM pictures. To limit the time available for nanotube growth, the target was located close to the front edge of the furnace ($d=10$ cm, Fig. 1) such that, after a known time spent at relatively uniform temperature, the plume would be thermophoretically drawn as rapidly as possible out the front of the

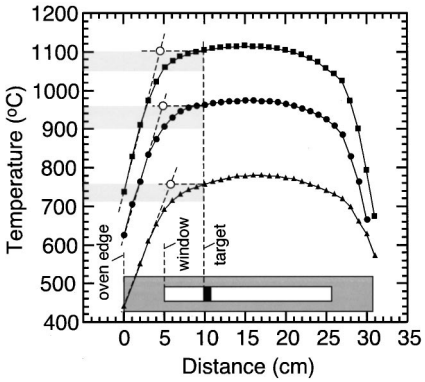

FIG. 2. Temperature profiles along the furnace axis measured at three different furnace temperatures: 780, 960, and 1100 °C at the center of the furnace. The inset at the bottom shows target and window edge positions relative to the oven edge at $d=0$. The open circle separates steep gradient and uniform temperature zones.

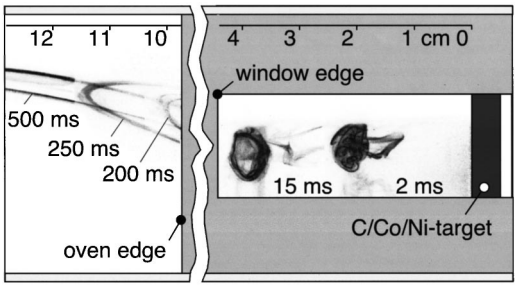

FIG. 3. Images of Rayleigh-scattered light (308-nm XeCl laser, 26 ns FWHM, 6 mJ/cm^2) from C/Ni/Co plume during synthesis of short SWNT's at 2 and 15 ms after ablation inside the furnace and at 200, 250, and 500 ms when the plume exits the furnace. The temperature at the target position was 760 °C. A Nd:YAG laser vaporizes a C/Ni/Co target inside a 2-in-diam quartz tube in 500 Torr Ar (flowing to the right at 100 sccm). Each image represents a different ablation event (5-ns gate width, opened simultaneously with the probing XeCl-laser pulse).

oven to deposit upstream on the wall of the quartz tube. Of utmost importance, however, was to assure that the plume spent a guaranteed time (10–20 ms) in the uniform-temperature region of the oven before it underwent the rapid cooling at the oven edge. Rayleigh-scattering images of the plume (in association with the measured temperature profiles of the oven) were used to measure and control this known growth time at uniform temperature. The ablated material was collected upstream on the wall of the quartz tube (collection point 1, Fig. 1).

Figure 2 shows the oven temperature profiles measured inside the quartz tube (along the central axis) under flowing gas conditions for three different oven temperature settings: 780, 960, and 1100 °C at the center of the furnace. The temperatures were uniform (within a 60–70 °C range) over the windowed region of the furnace and dropped rapidly within the final 5-cm region at both ends. To define the uniform temperature zones in Fig. 2, the target position defined the upper boundary ($d\sim 10$ cm), while the lower boundary ($d\sim 5$ cm) was determined at the distance where straight-line fits to the gradient regions of the temperature profiles intersected the constant temperature line at the target position. For the first 5 cm of plume travel (within the windowed region of the furnace between $d=5$ and 10 cm in Fig. 2) temperature variations at the three different oven temperatures used to grow the short SWNT's in this study were 760–715 °C ($\Delta T/T=5.9\%$), 960–900 °C ($\Delta T/T=6.2\%$), and 1100–1050 °C ($\Delta T/T=4.6\%$). However, during the next 5 cm of plume travel (from $d=0$ to 5 cm in Fig. 2) steep temperature gradients of ~70 °C/cm were used to stop the growth of SWNT's as the plume exited the oven.

To find the positions of the plume inside and outside the furnace we used Rayleigh-scattering imaging. Figure 3 shows images of the plume at 2 and 15 ms after ablation inside the furnace and at 200, 250, and 500 ms when the plume exits the furnace. Figure 4 shows more detailed dynamics of the plume within the furnace in the uniform-temperature zone. These images allow us to resolve the plume substructure within a vortex ring. One can see that this substructure is highly nonuniform. Many small turbulences can be seen within these vortex rings. The detailed description of the plume dynamics during SWNT growth was given in Refs. 17 and 18. Initially, the plume generates a strong shock front and traps itself between this shock front and the target. The forward-propagating plume sets the surrounding background gas in motion in such a way that it flows around the plume and forms vortices. These vortices trap the ejected material at later times after ablation. The confinement of the ejected material within the vortices and the small turbulences are very important for nanotube growth, since they greatly enhance the concentra-

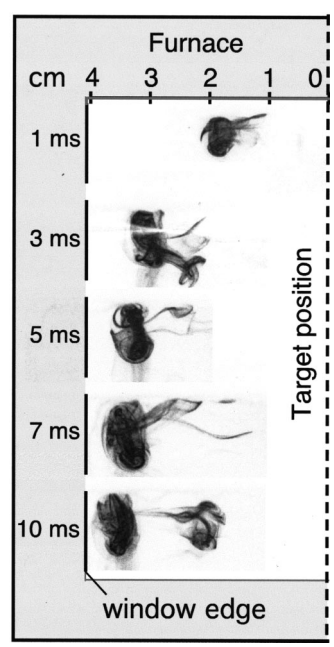

FIG. 4. Images of Rayleigh-scattered light from C/Ni/Co plume during synthesis of short SWNT's inside the furnace at 1–10 ms after ablation at 1100 °C.

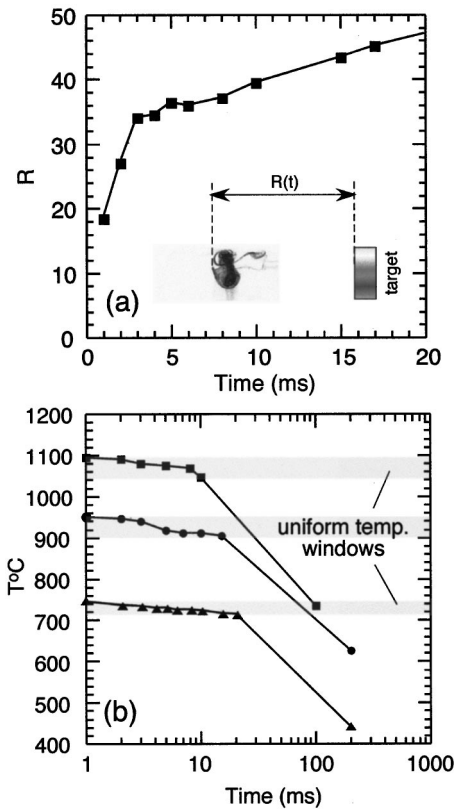

FIG. 5. (a) Distance of the leading edge of the plume from the target, R, vs time after ablation at $T=760\,°C$ at the target position. (b) Temperature encountered by the plume vs time after ablation at three different processing temperatures.

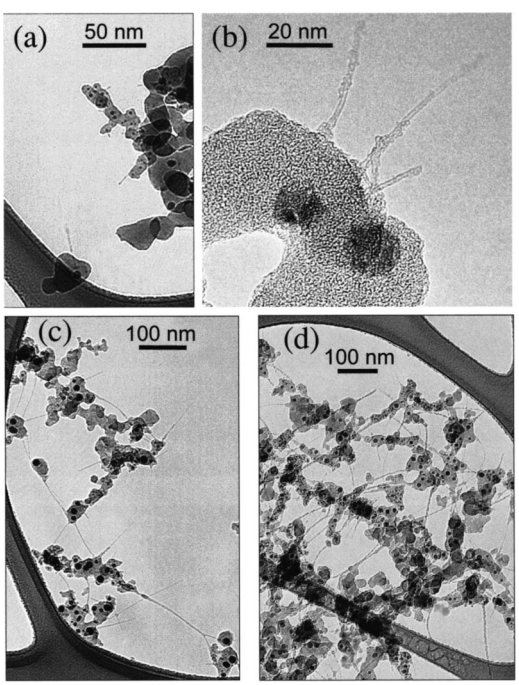

FIG. 6. TEM images of short SWNT's grown by laser vaporization at (a), (b) 760 °C, (c) 960 °C, and (d) 1100 °C. Note that the temperatures listed were measured inside the quartz tube at the target position.

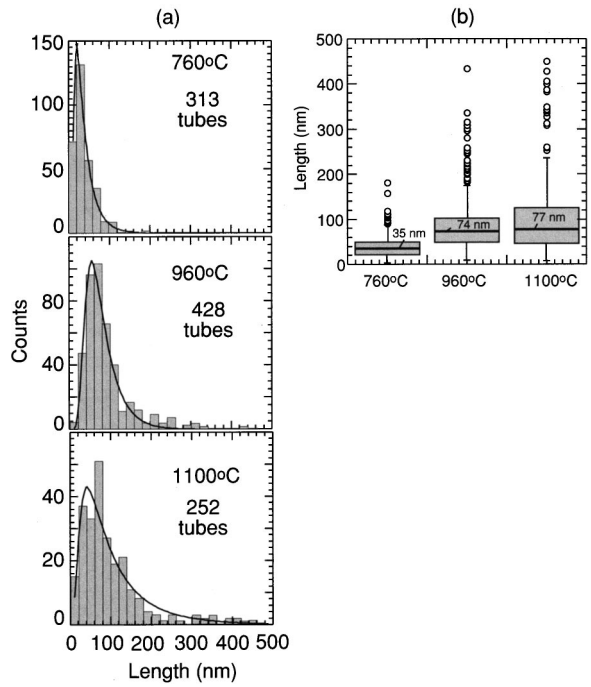

FIG. 7. (a) Length distribution of short SWNT's generated by the plume spending <200 ms inside the furnace at 760, 960, and 1100 °C. The curves represent a logarithmic normal distribution fits. (b) Statistical analysis of the length distribution presented by a 50% box plot. Boxes and bars include 50% and 90% of all measured tubes.

tion of the precursor material and the growth rate of carbon nanotubes.

In the uniform-temperature zone the shape of the vortex ring does not change much when it propagates forward. The diameter of the vortex ring usually increases slowly with time.[17,18] When the vortex ring approaches the temperature gradient zone its plane tilts relative to the tube axis and the ring elongates along this axis.[17,18] The plume exits the furnace in this tilted orientation to deposit onto the upper surface of the quartz tube (Fig. 3). To determine the temperature encountered by the propagating plume we measured the position of the leading edge of the plume at different times after ablation [Fig. 5(a)] and replotted this $R(t)$ curves as $T(t)$ using the oven temperature profiles, $T(R)$, shown in Fig. 2. Figure 5(b) shows the temperature encountered by the plume at different times after ablation at three different furnace temperatures. One can see that the ejected material spends approximately 10–20 ms at uniform temperature and 100–200 ms in the steep gradient zone.

Figures 6(a), 6(b), 6(c), and 6(d) show TEM images of short SWNT's synthesized at three different temperatures measured at the target position: 760 °C (a), (b), 960 °C (c), and 1100 °C (d). These images demonstrate that many short tubes grow from catalyst nanoparticles represented by small black dots in Fig. 6. In most cases we can easily see the ends of these short tubes and measure their length. High-resolution TEM (HRTEM) analysis of the 760 °C sample using HF-2000 FE TEM [Fig. 6(b)] demonstrated that the majority of the nanotubes observed in the lower-resolution

images are not bundles, but are short, individual SWNT's. Of 54 SWNT's measured by HRTEM, 45 were individual SWNT's, 8 double-SWNT bundles, and 1 triple-SWNT bundle.

Figures 7(a) and 7(b) show the length distributions, a regular histogram [Fig. 7(a)] and 50% box plot [Fig. 7(b)] for the SWNT's grown for restricted times at the three different oven temperatures. Boxes and bars in Fig. 7(b) include 50% and 90% of all measured SWNT's, respectively. The length distributions of short SWNT's in Fig. 7(a) were fitted with a logarithmic normal distribution. At higher furnace temperatures the maximum of the nanotube length distribution shifts to longer lengths and the width of the distribution increases. As shown in Fig. 7(b), at 760 °C the most probable length is 35 nm and 90% of all SWNT's are shorter than 90 nm. At 960 °C these values are 74 and 170 nm, and at 1100 °C they are 77 and 240 nm.

IV. PARTICLE TEMPERATURES INSIDE THE PROPAGATING VORTEX RING PLUME

It is important to measure the temperature of the particles in the propagating plume at different times after ablation. First, using this correlation we can estimate when SWNT's start to grow, since by this time the temperature should not exceed the eutectic temperature for carbon-metal catalyst mixture. It was shown experimentally that the yield of SWNT's drops rapidly at $T > T_{\mathrm{eut}}$ (C/Co, C/Ni).[24] Second, to limit the growth times and to estimate the growth rates of SWNT's it is necessary to determine how fast the species within the plume reach the ambient furnace temperature.

To estimate the temperature of carbon particles inside the propagating plume we measured their blackbody emission (incandescence) spectra at different times and positions in the furnace [Fig. 8(a)]. The plume emission spectra were fitted with the Planck blackbody function. The intensity of the blackbody emission from a particle of radius a at a wavelength λ into interval $\Delta\lambda$ is given by

$$I(\lambda,a)=\varepsilon(\lambda,a)8\pi^2a^2c^2h\Delta\lambda/\lambda^5[\exp(hc/\lambda k_BT)-1], \tag{1}$$

where $\varepsilon(\lambda,a)$ is the spectral emissivity and T is the absolute temperature of the particle. For small particles ($a < 0.3\lambda/2\pi$), $\varepsilon(\lambda,a)\sim 1/\lambda$ and $I(\lambda,a)\sim 1/\lambda^6$. For larger particles we can assume that $\varepsilon=\mathrm{const}$, which gives $I(\lambda,a)\sim 1/\lambda^5$. It should be mentioned that an ICCD detector counts photons: therefore, the ICCD signal is proportional to the number of photons per unit time, i.e., to $1/\lambda^4$ in the case of the constant emissivity ε.

Figure 8(b) shows an example of the blackbody fit of the emission spectrum of the carbon particles in the plume measured at $t=1$ ms after ablation assuming that $\varepsilon=\mathrm{const}$. This fit gives the plume temperature of 1488 °C. Figure 9(a) shows the temperature of the particles within the plume versus the time after ablation. The temperature of the plume approaches the ambient temperature (760 °C) after approximately 4 ms after ablation. For $T_{\mathrm{amb}}=1100$ °C, a plateau is observed at $T\sim 2500$ °C in the time interval 0.3–0.7 ms [Fig. 9(b)]. A similar plateau in the plume emission intensity was observed by Suzuki *et al.*[25] An exothermic process, probably formation of fullerenelike structures, keeps the plume temperature constant from 0.3 to 0.7 ms. In the case of higher ambient temperature (1100 °C), it is also takes approximately 4 ms after ablation for the particles within the plume to cool down to the ambient temperature.

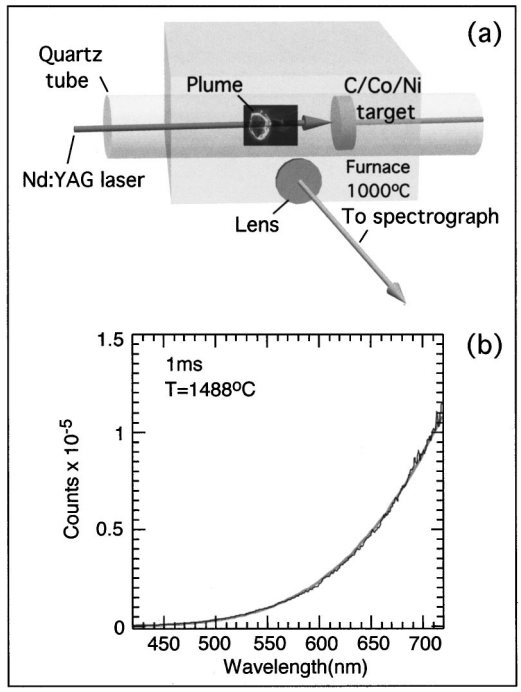

FIG. 8. (a) Schematic of the temperature measurements of the particles inside the propagating plume. (b) Experimental blackbody emission spectrum of carbon nanoparticles within the plume measured at 1 ms after ablation (dark curve) and fit to Planck's law, yielding a temperature of 1488 °C (light curve).

Particles in the plume cool by heat conduction to the surrounding buffer gas and by thermal radiation. In addition, the particles may undergo phase transition during the flight, such as vaporization or resolidification, e.g., conversion of amorphous carbon to SWNT's. The heating and cooling processes of small powder particles were considered theoretically in Refs. 26 and 27. The experimental $T(t)$ points shown in Fig.

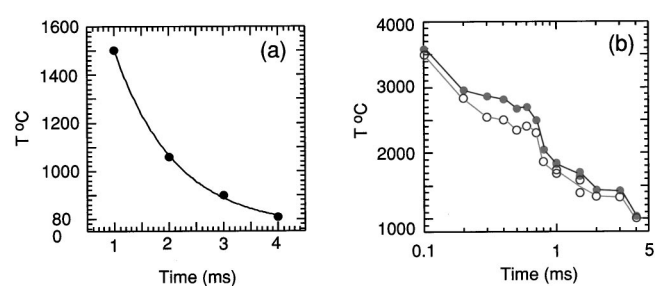

FIG. 9. Temperature of carbon particles inside the propagating plume vs time after ablation measured at different ambient temperatures: (a) 760 °C, $\varepsilon(\lambda,a)=\mathrm{const}$ (solid circles), the line shows the fit based on the Eq. (2); (b) 1100 °C, $\varepsilon(\lambda,a)=\mathrm{const}$ (solid circles), and $\varepsilon(\lambda,a)\sim 1/\lambda$ (open circles).

TABLE I. Lower and upper limits of the growth rates of SWNT's synthesized by nanosecond laser vaporization of a C/Co/Ni target.

Lower limit of growth rate				Upper limit of growth rate			
Oven temperature range (°C)	Time at $T>70$ °C (ms)	Most probable length (nm)	Growth rate (μm/s)	Uniform Oven temp. range (°C)	Time in uniform zone (ms)	Most probable length (nm)	Growth rate (μm/s)
760–700	25	35	1.4	760–715	20	35	1.8
960–700	100	74	0.7	960–900	15	74	5.0
1100–700	120	77	0.6	1100–1050	15	77	5.1

9(a) can be fitted fairly well using the simple assumption that the heat conduction to the background gas is the major process which decreases the temperature of the particles in the plume at $t>1$ ms. In this case,[26]

$$dT/dt=-A(T-T_{\text{oven}}). \tag{2}$$

The fit $T(t)=T_{\text{oven}}+T_0\exp(-At)$, derived from Eq. (2) to the experimental points in Fig. 9(a), gives $A=0.9$ 1/ms.

V. GROWTH RATES OF SWNT's

It is possible to estimate the growth rates of SWNT's in these experiments using the measured values of the most probable length of SWNT's (Fig. 7), the times the ablated material spent in the uniform temperature zones, and the short time (~4 ms) required to cool the particles within the plume down to the ambient temperature. The estimated growth rates are listed in Table I for the three ambient temperatures used in this study.

The lower and the upper limits of the growth rates were estimated using two different criteria. The lower limit was estimated on the basis of the minimum temperature at which the SWNT's can grow. Bandow *et al.*[13] estimated that the yield of SWNT's produced by nanosecond laser vaporization was about 3%–5% at $T=780$ °C. They did not find any SWNT's at room temperature. Sen *et al.*[28] concluded that the lowest threshold temperature for SWNT growth in the nanosecond laser ablation process is about 850 °C. Our study shows that short SWNT's can be synthesized for temperatures greater than 760 °C. To estimate the lower limit of the growth rate the minimum temperature for SWNT growth in nanosecond laser vaporization process was assumed to be about 700 °C, and the time spent by the ablated material at $T>700$ °C was estimated (Table I). The upper limit of the growth rate was estimated based on the time the vaporized material spent in the uniform-temperature zone. With these assumptions the average growth rates of SWNT's during these estimated time intervals are 0.6–5.1 μm/s.

The kinetics of noncatalytic carbon nanotube growth was studied using molecular dynamics and Monte Carlo simulations by Maiti *et al.*[29] In this study the fastest growth rates were estimated at different growth temperatures from 500 to 3000 K. For example, the growth rate was estimated as 82 μm/s at 1500 K. This value is $10-10^2$ times larger than the experimental values measured in this paper.

VI. RAMAN SPECTRA OF SHORT SWNT's

Figures 10 and 11 present Raman spectra of short SWNT's measured using the 632.8-nm (1.96-eV) line from a HeNe laser (Fig. 10) and the 514.5-nm (2.41-eV) line from an Ar^+ laser (Fig. 11). Figures 12(a) and 12(b) show a spectrum of a regular "long"-tube material synthesized at 1150 °C when the target was positioned near the center of the furnace. This spectrum was measured using an excitation wavelength of 632.8 nm (1.96 eV), which matches the energy separation between one-dimensional (1D) singularities in the first valence band and the first conduction band in metallic SWNT's, E_{11}^M.

The main feature of the tangential band of the long SWNT's around 1537 cm^{-1} [Fig. 12(b)] can be fitted with a Breit-Wigner-Fano (BWF) line shape.[30,31] This feature is typical for metallic SWNT's and originated from the lower-frequency A (A_{1g}) Raman component of the metallic tubes.

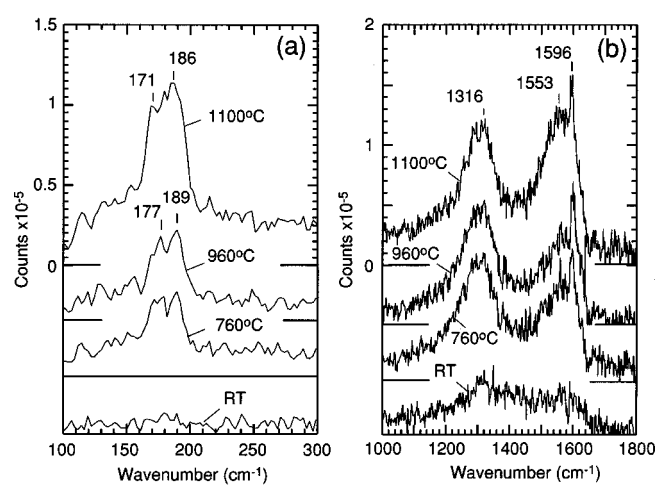

FIG. 10. Raman spectra of the (a) radial breathing mode and (b) the tangential stretching modes of short SWNT's generated at three different processing temperatures: 760, 960, and 1100 °C. The spectrum at the bottom was obtained for the material synthesized at room temperature when no tubes were produced. The excitation wavelength was 632.8 nm (1.96 eV).

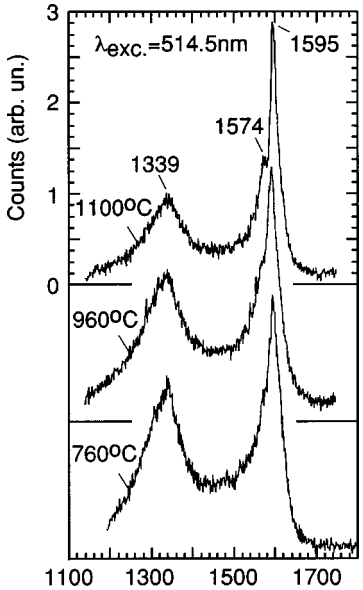

FIG. 11. Raman spectra of the tangential stretching modes of short SWNT's synthesized at three different processing temperatures: 760, 960, and 1100 °C. The laser excitation wavelength was 514.5 nm (2.41 eV).

The BWF line shape of this component is due to coupling of the discrete phonons to an electronic continuum.[30,31] The higher-frequency A (A_{1g}) metallic component around 1578 cm^{-1} is not coupled to the electronic continuum and has a Lorentzian line shape. Only these two Raman components are required to fit the tangential band of metallic SWNT's because of their strong enhancement due to electromagnetic effect.[31] The peak around 1594 cm^{-1} is related to semiconducting nanotubes. This feature is typical for semiconducting tubes and appears probably because of the laser resonance with the energy separation between 1D singularities in the $3d$ valence and the $3d$ conduction bands, $E_{33}^{S}(d_t)$, for the larger tube diameters d_t.[32] The semiconducting tangential band can be fitted with three major components. The fitting parameters are listed in Table II. The radial breathing mode

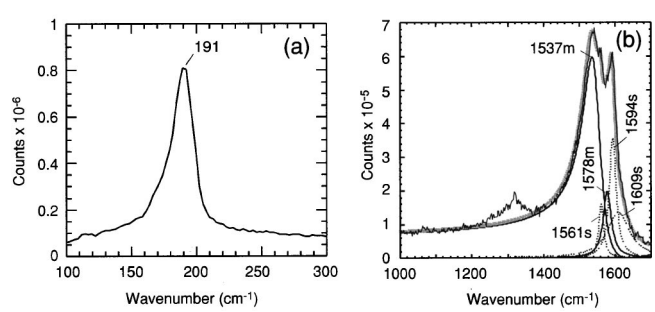

FIG. 12. (a) Raman spectrum of the tangential stretching mode of normal long SWNT's produced at 1150 °C when the target was positioned at $d=20$ cm from the front of the furnace and the ejected material was collected at point 2 on the collector (see Fig. 1). (b) Line shape analysis of the tangential G band measured using a 632.8-nm (1.96-eV) HeNe laser. The fit parameters are listed in Table II.

TABLE II. Line shape analysis of the tangential Raman band measured using a 632.8-nm (1.96-eV) HeNe laser. The lower-frequency metallic feature around 1537 cm^{-1} was fitted with the BWF line shape, $I(\omega)=I_0[1+(\omega-\omega_{BWF})/q\Gamma]^2/1+[(\omega-\omega_{BWF})/\Gamma]^2$. In addition, the higher-frequency metallic (M) band around 1578 cm^{-1} and three semiconducting (S) bands with a Lorentzian shape were used to fit the tangential Raman band. The weak semiconducting E_2 (E_{2g}) band around 1550 cm^{-1} was not included in this fit.

Symmetry	ω (cm^{-1})	Γ (cm^{-1})	$1/q$
$A(A_{1g})$	1545^M	29	−0.32
$A(A_{1g})$	1561^S	8	
$A(A_{1g})$	1578^M	14	
$A(A_{1g})$	1594^S	11	
$E_2(E_{2g})$	1609^S	37	

(RBM) for the long tubes shows a peak at 191 cm^{-1} and a shoulder around 170 cm^{-1} [Fig. 12(a)].

The short SWNT's show the same main Raman peaks as the long tubes. The radial breathing band of the short tubes consists of two unresolved peaks at 186 and 171 cm^{-1} [Fig. 10(a)]. The absolute intensity of these peaks decreases as the processing temperature drops. The soot generated at room temperature does not show any RBM features, since no tubes can be grown at room temperature by nanosecond laser vaporization. The tangential Raman mode shows two peaks at 1553 and 1586 cm^{-1} [Fig. 10(b)] that can be assigned to metallic and semiconducting SWNT's, respectively. The metallic feature at 1553 cm^{-1} disappeared when the excitation wavelength was shifted to the semiconducting "window," $\lambda=514.5$ nm (2.41 eV). In this case two regular A (A_{1g}) components of the semiconducting tubes were observed (Fig. 11). However, in the case of short tubes, a strong disorder-induced peak around 1316 cm^{-1} ($\lambda_{exc}=632.8$ nm) or 1339 cm^{-1} ($\lambda_{exc}=514.5$ nm) was observed [Figs. 10(b) and 11]. To understand the contribution of the amorphous carbon material in our samples to the so-called disorder-induced band (or D band) we measured the Raman spectra at room processing temperature when no tubes were synthesized [Figs. 10(a) and 10(b)]. In this case, we observed a broad double-peak feature that is typical for amorphous carbon material.[33] The absolute intensity of the D band in the case of amorphous carbon soot synthesized at room temperature is much lower compared to that for the short SWNT's containing soot produced at elevated temperatures [Fig. 10(b)]. Probably the finite size ($<\lambda_{exc}$) of the short tubes results in strong contribution to the D band in addition to the contribution from the amorphous carbon.

The Raman spectra of short tubes show that they are well formed structurally. The effects of finite length on the electronic structure of carbon nanotubes were considered theoretically in Ref. 34. As the length of the SWNT's increases, the density of states spectrum of SWNT's changes from that characteristic of a 0D system to that typical of a 1D system. As was shown in Ref. 34, this transformation was completed for SWNT's about 10 nm long.

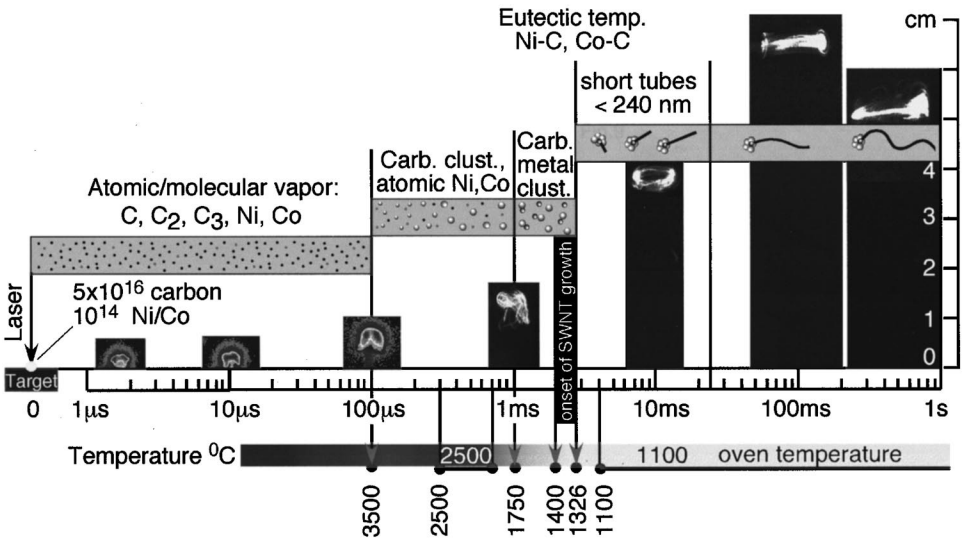

FIG. 13. Summary of the results from the *in situ* imaging and spectroscopic diagnostic investigations of SWNT's growth inside a hot oven. Actual images of the laser plasma ($t<200$ μs) and Rayleigh-scattering images of the plume ($t>200$ μs) are shown vs time (scale in cm at right). During the first 100 μs after ablation, the laser plasma is very hot, and emission from excited atoms and molecules dominate LIF from ground-state species. Ground-state populations then peak and subsequently disappear due to condensation. Images and LIF spectra show that carbon condenses by $t=200$ μs after ablation, while the metal catalyst atoms condense much later. The ground-state atomic Co population is maximum at $t=0.8$ ms and then condenses by $t=2$ ms. By $t=2$ ms, no LIF is detectable, only LIL and RS from clusters and nanoparticles (i.e., nearly all atoms and molecules have converted into clusters and nanoparticles, as evidenced by the vortex ring structure of the plume). At $t=2$ ms, the plume temperature is $\sim$1400 °C, just above the Ni/C and Co/C eutectic temperatures (note that Ni/C and Co/C eutectic temperatures are slightly lower for nanoparticles compared to the bulk material). By $t=4$ ms, the plume has thermalized to the oven temperature. If growth is stopped at $t\sim25$ ms, only short nanotubes are found (<240 nm in length), indicating that the majority of growth takes place over much longer times.

VII. SUMMARY: THE SEQUENCE OF EVENTS IN SWNT GROWTH BY THE LASER-VAPORIZATION METHOD

In conclusion, we discuss a comprehensive picture of the events in the laser-ablation method leading to SWNT growth by combining the results of this study with the results of our previous works on plume dynamics and spectroscopy, described in Refs. 17, 18, and 35.

Figure 13 summarizes the results of our *in situ* spectroscopic diagnostics using time, spatial, and temperature coordinates. Initially a Nd:YAG laser pulse produces atomic-molecular vapor containing $\sim5\times10^{16}$ carbon and $\sim10^{14}$ Ni/Co atoms as estimated by weighing the C/Ni/Co target before and after laser ablation. The evaporated material stays in the vapor phase until approximately 100 μs after ablation.[17,18] During this time, the laser plasma is very hot and emission from excited atoms and molecules dominate laser-induced emission from ground-state species. The laser plasma cools rapidly, increasing the populations of the atomic and molecular ground states as indicated by laser-induced fluorescence (LIF) measurements.

To observe the plume of ejected material at $t>200$ μs we used laser-induced incandescence and Rayleigh scattering from clusters and nanoparticles. By that time the plume becomes substantially nonuniform, as can be seen from the Rayleigh-scattering images (Figs. 3, 4, and 13) demonstrating pronounced turbulent structure within the plumes. At later times (>2 ms) the plume aquires a characteristic vortex ring shape that still has a highly turbulent substructure (Figs. 3, 4, and 13).

Images of the plume and LIF spectra show that carbon condenses and forms clusters by $t=200$ μs after ablation, while the metal catalyst atoms condense much later. The ground-state atomic Co population is maximum at $t\sim0.8$ ms, and then $\sim$90% of cobalt atoms condense into clusters by $t\sim2$ ms.[17,18]

The Mie theory interpretation of the extinction spectra (absorption plus scattering[35]) shows that the size of the carbon particles within the plume at these times does not exceed 20 nm at ambient temperatures $\sim$1100 °C. However, at lower ambient temperatures ($\sim$760 °C) much larger aggregates were observed. Using Mie theory for spherical particles, the size of these aggregates was estimated as $\sim$80 nm.[35] This rapid aggregation of carbon nanoparticles at lower processing temperatures results in a decrease in mobility and could be one of the reasons for the rapid decrease of SWNT yields at lower ambient temperatures.

The temperature measurements in this study permit an estimate for the onset of SWNT growth. At $t=2$ ms the plume temperature is $\sim$1400 °C, just above the Ni/C and Co/C eutectic temperatures. Since it is well known that the yield of SWNT's drops rapidly at $T>T_{\mathrm{eut}}$,[7,24] we can estimate the onset of SWNT growth as $\sim$2 ms for our experimental conditions. By this time, we have shown that the majority of the ejected vapor has already condensed into

clusters and nanoparticulate aggregates, so SWNT nucleation appears to occur in this environment.

In order to confirm where the majority of SWNT growth occurs and estimate growth rates, plume imaging and steep temperature gradients near the end of the furnace were employed to restrict the growth times of SWNT's to about 15–20 ms at high temperature in the uniform region of the oven. Very short SWNT's forming thin bundles consisting of a few tubes were found to have most probable lengths of 35–77 nm depending on the processing ambient temperature 760–1100 °C. This permits upper and lower limits for the growth rate of SWNT's to be estimated as ~0.6 and 5.1 μm/s, respectively. Short SWNT's were synthesized and characterized by TEM and Raman spectroscopy. The Raman spectra of the short tubes show that they are well formed structurally.

However, the main conclusions of these time-resolved growth studies are that the majority of SWNT growth occurs for times longer than 20 ms after laser vaporization through the conversion of condensed-phase carbon and metal catalyst clusters and nanoparticles.

ACKNOWLEDGMENTS

The authors gratefully acknowledge the assistance of M.A. Guillorn, P.F. Britt, and S.J. Pennycook. This research was sponsored by the U.S. Department of Energy under Contract No. DE-AC05-00OR22725 with the Oak Ridge National Laboratory, managed by UT-Battelle, LLC, and the Laboratory-Directed Research and Development Program at ORNL.

*Present address: Center for Advanced Microscopy, Michigan State University, East Lansing, Michigan 48824.

[1] B. T. Yakobson and R. E. Smalley, Am. Sci. **85**, 324 (1997).
[2] T. Guo, P. Nikolaev, A. Thess, D. T. Colbert, and R. E. Smalley, Chem. Phys. Lett. **236**, 419 (1995).
[3] A. Thess, R. Lee, P. Nikolaev, H. Dai, P. Petit, J. Robert, C. Xu, Y. H. Lee, S. G. Kim, A. G. Rinzler, D. T. Colbert, G. E. Scuseria, D. Tomanek, J. E. Fisher, and R. E. Smalley, Science **273**, 483 (1996).
[4] M. Yudasaka, T. Ichihashi, T. Komatsu, and S. Iijima, Chem. Phys. Lett. **299**, 91 (1999).
[5] A. G. Rinzler, J. Liu, H. Dai, P. Nikolaev, C. B. Huffman, F. J. Rodriguez-Macias, P. J. Boul, A. H. Lu, D. Heymann, D. T. Colbert, R. S. Lee, J. E. Fisher, A. M. Rao, P. C. Eklund, and R. E. Smalley, Appl. Phys. A: Mater. Sci. Process. **67**, 29 (1998).
[6] M. Yudasaka, T. Ichihashi, and S. Iijima, J. Phys. Chem. B **102**, 10201 (1998).
[7] A. A. Gorbunov, R. Friedlein, O. Jost, M. S. Golden, J. Fink, and W. Pompe, Appl. Phys. A: Mater. Sci. Process. **69**, S593 (1999).
[8] A. C. Dillon, P. A. Parilla, J. L. Alleman, J. D. Perkins, and M. J. Heben, Chem. Phys. Lett. **316**, 13 (2000).
[9] A. C. Dillon, P. A. Parilla, K. M. Jones, G. Riker, and M. J. Heben, in *Advances in Laser Ablation of Materials*, edited by R. K. Singh, D. H. Lowndes, D. B. Chrisey, E. Fogarassy, and J. Narayan, Mater. Res. Soc. Symp. Proc. No. 526 (Materials and Research Society, San Francisco, 1988), p. 403.
[10] M. Yudasaka, R. Yamada, N. Sensui, T. Wilkins, T. Ichihashi, and S. Iijima, J. Phys. Chem. B **103**, 6224 (1999).
[11] O. Jost, A. A. Gorbunov, J. Moller, W. Pompe, A. Graft, R. Friedlein, X. Liu, M. S. Golden, and J. Fink, Chem. Phys. Lett. **339**, 297 (2001).
[12] M. Yudasaka, T. Komatsu, T. Ichihashi, Y. Achiba, and S. Iijima, J. Phys. Chem. B **102**, 4892 (1998).
[13] A. S. Bandow, S. Asaka, Y. Saito, A. M. Rao, L. Grigorian, E. Richter, and P. C. Eklund, Phys. Rev. Lett. **80**, 3779 (1998).
[14] S. Arepalli and C. D. Scott, Chem. Phys. Lett. **302**, 139 (2001).
[15] F. Kokai, K. Takahashi, M. Yudasaka, R. Yamada, T. Ichihashi, and S. Iijima, J. Phys. Chem. B **103**, 4346 (1999).
[16] D. B. Geohegan (unpublished).
[17] A. Puretzky, D. B. Geohegan, X. Fan, and S. J. Pennycook, Appl. Phys. Lett. **76**, 182 (2000).
[18] A. A. Puretzky, D. B. Geohegan, X. Fan, and S. J. Pennycook, Appl. Phys. A: Mater. Sci. Process. **70**, 153 (2000).
[19] D. B. Geohegan, H. Schittenhelm, X. Fan, S. J. Pennycook, A. A. Puretzky, M. A. Guillorn, D. A. Blom, and D. C. Joy, Appl. Phys. Lett. **78**, 3307 (2001).
[20] F. Kokai, K. Takahashi, M. Yudasaka, and S. Iijima, J. Phys. Chem. B **104**, 6777 (2000).
[21] G. De Boer, S. Arepalli, W. Holmes, P. Nikolaev, C. Range, and C. Scott, J. Appl. Phys. **89**, 5760 (2001).
[22] S. Arepalli, P. Nikolaev, W. Holmes, and B. S. Files, Appl. Phys. Lett. **78**, 1610 (2001).
[23] C. D. Scott, S. Arepalli, P. Nikolaev, and R. E. Smalley, Appl. Phys. A: Mater. Sci. Process. **72**, 573 (2001).
[24] H. Kataura, Y. Kumazawa, Y. Maniwa, Y. Ohtsuka, R. Sen, S. Suzuki, and Y. Achiba, Carbon **38**, 1691 (2000).
[25] S. Suzuki, H. Yamaguchi, T. Ishigaki, R. Sen, H. Kataura, W. Kratschmer, and Y. Achiba, Eur. Phys. J. D **16**, 369 (2001).
[26] C. J. Dasch, Appl. Opt. **23**, 2209 (1984).
[27] Y. P. Wan, V. Prasad, G. X. Wang, S. Sampath, and J. R. Fincke, J. Heat Transfer **121**, 691 (1999).
[28] R. Sen, Y. Ohtsuka, T. Ishigaki, D. Kasuya, S. Suzuki, H. Kataura, and Y. Achiba, Chem. Phys. Lett. **332**, 467 (2000).
[29] A. Maiti, C. J. Brabec, C. Roland, and J. Bernholc, Phys. Rev. B **52**, 14 850 (1995).
[30] H. Kataura, Y. Kumazawa, Y. Maniwa, I. Umezu, S. Suzuki, Y. Ohtsuka, and Y. Achiba, Synth. Met. **103**, 2555 (1999).
[31] S. D. M. Brown, A. Jorio, P. Corio, M. S. Dresselhaus, G. Dresselhaus, R. Saito, and K. Kneipp, Phys. Rev. B **63**, 155414 (2001).
[32] S. D. M. Brown, P. Corio, A. Marucci, M. S. Dresselhaus, M. A. Pimenta, and K. Kneipp, Phys. Rev. B **61**, R5137 (2000).
[33] M. J. Matthews, M. A. Pimenta, M. S. Dresselhaus, G. Dresselhaus, and M. Endo, Phys. Rev. B **59**, R6585 (1999).
[34] A. Rochefort, D. R. Salahub, and P. Avouris, J. Phys. Chem. B **103**, 641 (1999).
[35] A. A. Puretzky, D. B. Geohegan, C. H. Schittenhelm, X. Fan, and M. A. Guillorn, Appl. Surf. Science (to be published).